LANGMUIR

pubs.acs.org/Langmuir Article

Ultrafast Joule Heating Modification of Methane-Pyrolyzed Carbon Black for Supercapacitor Application

Guinan He, Zhongjie Shen,* and Haifeng Liu*

Cite This: https://doi.org/10.1021/acs.langmuir.4c03818 Read Online

ACCESS | Metrics & More | Article Recommendations

ABSTRACT: Carbon black from methane pyrolysis for hydrogen is an alternative resource and can be improved for conductive material supplication. Our current work uses an ultrafast Joule heating technique to modify the methane-pyrolyzed carbon black and prepare nanoparticles of electrode material for supercapacitor application, coupled with density functional theory, structural, and electrochemical analyses. Evolution rules of the carbon and pore structures of the modified sample with an increase in temperature reveal good structure improvements. The graphitization degree of modified carbon black nanoparticles increases, and the particle morphology changes from a smooth surface, disordered structure removal, and pore formation to graphite crystallization. Band structure and state density analytical results show that the modified carbon black with a defect-free structure possesses metallic properties and exhibits good electrical conductivity. A temperature around 1576 °C to the initial graphitization was defined based on the critical point of the evolution of ordered and disordered structures, while the electrical conductivity of the carbon black nanoparticles at 2000 °C reaches 2300 S/m. The modified carbon black performed with stable charge/discharge characteristics, exhibiting a 4.31% capacitance drop at a current load of 2 A/g and a 18.31% capacitance drop at a current load of 20 A/g.

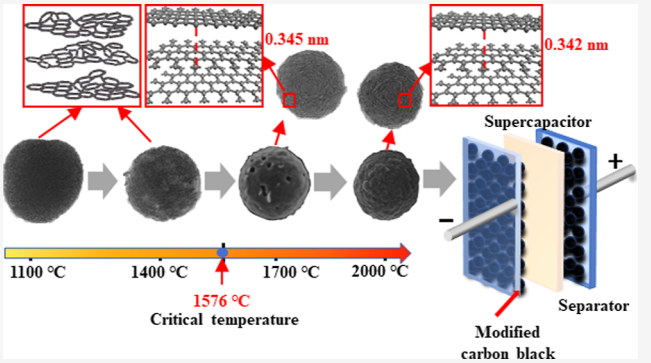

1. INTRODUCTION

Renewable energy, as a key role on the action of the carbon emission reduction and green development of global energy sector, is being received wide attention and utilized in many fields, such as solar, hydro, wind energy, etc.[1,2] These renewable energies are influenced by naturality (e.g., fluctuating seasonal and regional properties), which significantly limit the stable and large-scale utilization.[3] To solve these issues, supercapacitors as an energy storage technology, with high power density, maintenance-free, long life, and other excellent performance become the focus of academic and industrial attention.[4−6] Supercapacitor technology has made rapid progress, especially in the academic field, and new technological breakthroughs have been reported, with the support and great progress in manufacturing and application, including communications, urban rail transit systems, intelligent distributed power grids, and military equipment.[7−9]

Carbon black, which has good conductivity and compatibility with other materials (such as conductive polymers), is a promising material for manufacturing carbon electrodes in the supercapacitor.[10] Compared with the carbon black prepared from acetylene, tar residue, coal, or other resources, the byproduct carbon black from the methane pyrolysis (MP), of which the main target is hydrogen production, is a low-cost material and can be modified for a high value.[11] In some industrial applications, the MP reaction also occurs as a side reaction in the recovery of high-temperature flue gas from methane. However, due to the high temperature of the flue gas, a large amount of carbon black is generated during the reforming process, which may lead to catalyst deactivation due to carbon deposition.[12] Therefore, catalysts are generally not added in these fields, and higher temperatures are often required for the flue gas to react fully with methane, exceeding 1100 °C to ensure that the MP and reforming reactions proceed sufficiently, resulting in a methane conversion rate of over 90%.[13] The primary products of MP are large-particle-sized amorphous carbon or carbon with graphite-like properties, which are deficient in organic functional groups that enhance surface reactivity and exhibit high thermal stability.[14] Nonetheless, the amorphous structure and relatively low specific surface area of the byproduct carbon black restrict further application in the supercapacitor field.[15] The

Received: September 27, 2024
Revised: November 28, 2024
Accepted: November 28, 2024

modification of the methane-pyrolyzed carbon black is an alternative method to advance the charge specific volume and conductivity.

Ordered structures of the carbon black typically exhibit better electron mobility.[16] Graphitization modification enables the effective transformation of carbon black from an amorphous structure into an ordered one, which can significantly enhance the electrical conductivity of carbon black, thereby accelerating the charging and discharging rates of supercapacitors.[17] Considering that carbon black possesses carbon-based properties and exhibits physical and chemical characteristics similar to graphite, the transformation into a more structured material is feasible.[18] Compared to oxidation and doping modifications, high-temperature thermal treatment more efficiently enhances the electrical conductivity of carbon black while avoiding structural damage that may result from excessive oxidation or doping.[19] The high-temperature graphitization process includes the stages of carbonization and graphitization, where the temperature for graphitization is typically above 2000 °C.[20] Through the application of high-temperature thermal treatment, the carbon particles within the carbon black are induced to reorganize.[21] Such reorganization converts a shift from amorphous state to a crystalline arrangement in the formation of a graphite-like structure, improving the electrical conductivity.[22] However, the graphitization process induced by high temperature varies among different substances and across different forms of the same substance, attributable to the distinct initial configurations of carbon atoms and the prevalence of lattice defects.[23] For instance, highly active carbonaceous materials like activated carbon exhibit a more loosely packed arrangement of carbon atoms, necessitating temperatures exceeding 2500 °C for the graphitization process to facilitate the transition into an ordered graphite structure.[24] In contrast, the commercial high-temperature graphitization process typically requires the temperature reaching 3000 °C.[25] Therefore, the study of the process of carbon black graphitization has always been one of the core issues of carbon black graphitization.

Recently, the ultrafast Joule heating technology has been reported as a method that saves time and energy and has become a strong candidate for carbon black graphitization methods.[26] Ultrafast Joule heating technology enables rapid temperature increase and decrease, capable of generating high temperatures in high-resistance areas.[27] This capability effectively repairs the intrinsic structural defects of carbon materials, leading to efficient graphitization.[28] Additionally, ultrafast Joule heating technology can be widely applied to the graphitization treatment of various precursors, such as bowl-like carbon,[29] biochar,[30] and commercial carbon black.[31] This technology effectively mitigates issues like surface oxidation, agglomeration, and immiscibility, which are commonly encountered during the preparation process of nanomaterials.[32] However, research on the high-temperature graphitization of methane-pyrolyzed carbon black, which has low reactivity, is currently relatively scarce. Therefore, further in-depth study of the high-temperature graphitization process of methane-pyrolyzed carbon black is warranted.

In this study, ultrafast Joule heating technology was used to conduct high-temperature structural modification experiments on methane-pyrolyzed carbon black. Instruments such as an X-ray spectrometer, a transmission electron microscope, and a multifunctional physical property measurement system were used to characterize the structure of the synthesized and modified carbon black. Density functional theory (DFT) calculations were combined to simulate the impact of carbon black defects on electrical conductivity during the high-temperature graphitization process. A systematic study of the relationship between the microstructure of the carbon black samples and the high-temperature conditions is conducted, with particular attention given to the variation patterns of the carbon black graphitization degree. Finally, the performance of modified carbon black in supercapacitors was tested and verified by using an electrochemical workstation.

2. EXPERIMENTS AND SIMULATION

2.1. Materials. The carbon black sample was prepared by using the chemical vapor deposition method of MP (CH_4, purity 99.9%) in a tubular furnace. The pyrolysis temperature was set at 1100 °C, and the flow rate of the methane gas was set to 300 mL/min with ambient pressure. After cooling to room temperature in the tube furnace, the deposited carbon black at the bottom of the tube furnace was collected, denoted as C_1-x, where C_1 represents the carbon black deposited in the tube furnace, and x represents the reaction temperature in degrees Celsius. Fully automatic proximate analyzer (Changsha Kaiyuan Instruments, 5E-MACIII and 5E-MVC6700, China) was utilized to characterize the purity of the carbon black. The result is shown in Table 1.

Table 1. Carbon Black Information Used in This Study

	proximate analysis (ad, wt %)				
	moisture (M)	volatiles (V)	fixed carbon (FC)	ash (A)	particle size (nm)
C_1-1100	0.86	7.48	91.38	0.28	500

2.2. High-Temperature Modification Experiment. The collected carbon black (0.2 g) was spread in a graphite boat and placed in an ultrafast Joule heating device. The device diagram is shown in Figure 1. After the furnace chamber had been continuously

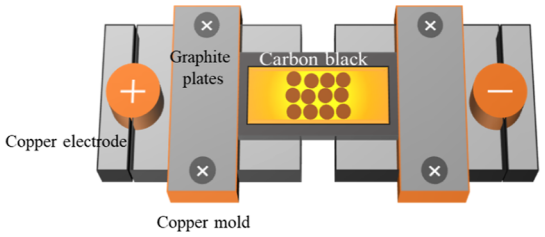

Figure 1. Diagram of the ultrafast Joule heating device.

evacuated three times, the carbon black was rapidly heated to 1400 °C, 1700 °C, and 2000 °C at a heating rate of 100 °C/s for thermal modification and held the temperature for 10 s before quickly annealing and cooling. After cooling to room temperature in the furnace, we introduced argon gas to retrieve the modified carbon black sample. The resulting product was named C_2-x, where C_2 represents the carbon black modified by an ultrafast Joule heating device.

2.3. Structural Characteristic Analysis. The crystal structure of carbon black was analyzed using an X-ray diffractometer (Thermo Fisher Scientific, America) with Cu Kα radiation, within a 2θ range of 10°−80° at a scanning rate of 2°/min. The interlayer spacing (d_{002}) was calculated based on the Bragg equation, as described by eq 1. The average crystal size of the carbon black was calculated using the Debye−Scherrer equation, indicated by eq 2.[33] The determination of the crystallite thickness (L_c) and lateral size (L_a) employed K-values of 0.9 and 1.84, respectively, where L_c represents the thickness perpendicular to the basal plane obtained from the (002) reflection, and L_a represents the thickness parallel to the basal plane obtained

https://doi.org/10.1021/acs.langmuir.4c03818
Langmuir XXXX, XXX, XXX−XXX

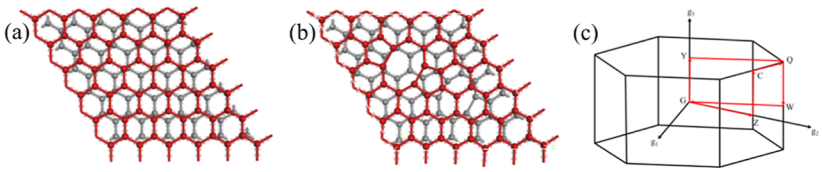

Figure 2. Optimized carbon black structure and band integration path. (a) Optimized electronic structure of defect-free carbon black. (b) Optimized electronic structure of double-vacancy defect carbon black. (c) High symmetry points in Brillouin region.

from the (100) reflection. Additionally, the carbon black structure was further tested using a Raman spectrometer (Thermo Fisher Scientific, America) with an incident laser power of 4 mW at a wavelength of 532 nm.

$$d_{002} = \lambda/(2\cdot\sin\theta) \quad (1)$$

where λ represents the wavelength of X-rays, 1.54 Å, and θ is Bragg diffraction angle, degrees.

$$L = K\cdot\lambda/(\beta\cdot\cos\theta) \quad (2)$$

where K is the Scherrer constant and β is the half-height width of the diffraction peak, radians.

The specific surface area and pore size distribution of the carbon black samples were characterized by using a nitrogen adsorption/desorption analyzer (Quantachrome Corp, USA). The surface morphology and internal structural feature of carbon black were tested using field emission scanning electron microscopy (FESEM) (GeminiSEM 500, Germany) and transmission electron microscopy (TEM) (Talos F200X, America), respectively.

The electrical conductivity (σ) of the carbon black samples was assessed by utilizing a powder resistivity tester (FT-300I, China) under pressures ranging from 5 to 25 MPa. The conductivity of samples was calculated based on resistance and sample dimensions (length and cross-sectional area) using the following formula[34]

$$\sigma = L/(R\cdot S) \quad (3)$$

where R represents the electrical resistance of the sample, Ω, S denotes the cross-sectional area of the sample, m^2, and L is the length of the sample, m.

2.4. Electrochemical Properties. Electrochemical tests were conducted in a three-electrode cell in 1 M H_2SO_4, with carbon black mixed with anhydrous ethanol and poly(tetrafluoroethylene) prepared on a rotating disk electrode to make the working electrode. The carbon black loading was 0.7 mg/cm^2. A platinum electrode was used as the counter electrode, and an Ag/AgCl electrode was used as the reference electrode.[34]

Cyclic voltammetry tests were carried out on a Pine electrochemical workstation in the United States with a scan rate of 100 mV/s. The initial and final voltages for the tests were set at 0 and 0.8 V, respectively. Constant current charge−discharge cycling tests were performed at current densities of 0.5−2 A·g^{-1} and 20 A·g^{-1}. The specific capacitance of different carbon black samples was calculated based on the discharge process of the constant current charge−discharge curves, using the following formula[34]

$$C = I\cdot\Delta t/(m\cdot\Delta U) \quad (4)$$

where I denotes the discharge current in amperes, A, Δt signifies the discharge time in seconds, s, m represents the mass of the carbon black sample loaded in grams, g, and ΔU indicates the discharge voltage range in volts, V.

2.5. DFT Analysis. As a widely recognized and successful method in the realms of condensed matter physics, quantum chemistry, and computational physics,[35] DFT serves as an effective tool for elucidating the intricate relationship between the electrical conductivity variations of carbon black and underlying electronic structure. Utilizing the CASTEP software package within the Materials Studio software suite, computational analyses were conducted on both pristine and double-vacancy-defective structures of carbon black to ascertain the relationship between defects and electrical conductivity. The generalized gradient approximation was applied to modify the PBE functional for addressing exchange-correlated potential energy.[36] The energy cutoff point was set to 400 eV, and the k point was set to 20 × 20 × 2. In the calculation process, by expanding the graphene primitive cell into a 5 × 5 × 2 super cellular structure, the defect free and double-vacancy defect carbon black model were established. The optimized carbon black structure and band integration path are depicted in Figure 2. The calculation path was set as G → W → Q → Y → G → Z → C → Q to calculate the band structure and state density distribution of carbon black with different defect degrees.

3. RESULTS AND DISCUSSION

3.1. Temperature Effect on Carbon Structure. The XRD spectra for the modified carbon black samples C_1-1100, C_2-1400, C_2-1700, and C_2-2000 are illustrated in Figure 3. The 002 peak of the carbon black sample prepared at 1100 °C is clearly broad, indicating low crystalline carbon. Upon an increase in temperature, 002 peaks sharpen and narrow, signifying an enhanced structural order within carbon black. The structural parameters of various carbon black samples, as calculated and detailed in Table 2, show that as the temperature increases, the interlayer spacing d_{002} decreases from 0.349 nm to 0.342 nm, gradually approaching the

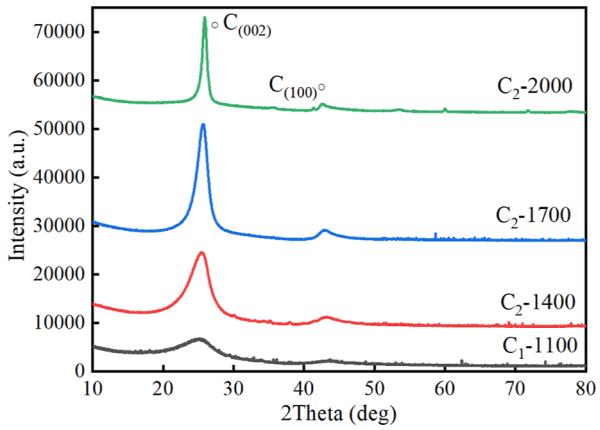

Figure 3. XRD spectra of modified carbon black samples at different temperatures.

Table 2. XRD Structure Parameters of Carbon Black at Different Temperatures

sample	C_1-1100	C_2-1400	C_2-1700	C_2-2000
2θ (002)/°	25.478	25.525	25.759	25.993
2θ (100)/°	43.521	43.451	43.143	42.786
fwhm (002)	4.325	3.727	1.976	0.891
fwhm (100)	4.211	3.216	2.488	1.143
d_{002}/nm	0.349	0.348	0.345	0.342
L_c/nm	1.863	2.162	4.080	9.053
L_a/nm	4.155	5.439	7.023	15.268

https://doi.org/10.1021/acs.langmuir.4c03818
Langmuir XXXX, XXX, XXX−XXX

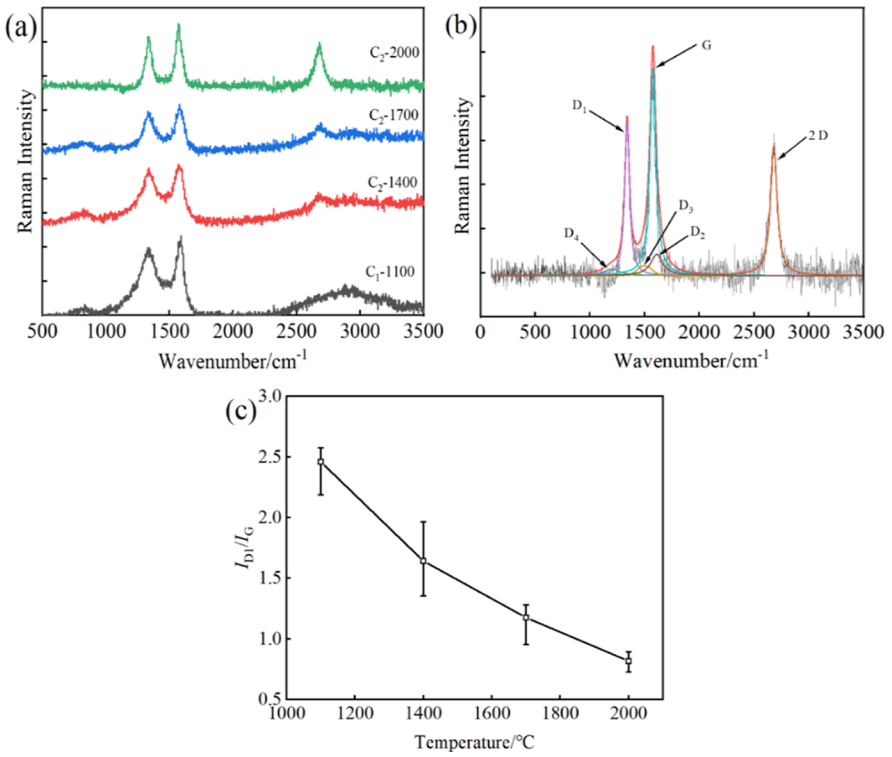

Figure 4. Raman spectroscopy of ordered structure variations in carbon black at different temperatures. (a) Raman spectra. (b) Raman spectrum fitting diagram of C_2-2000. (c) I_{D1}/I_G ratio changes of carbon black samples at different temperatures.

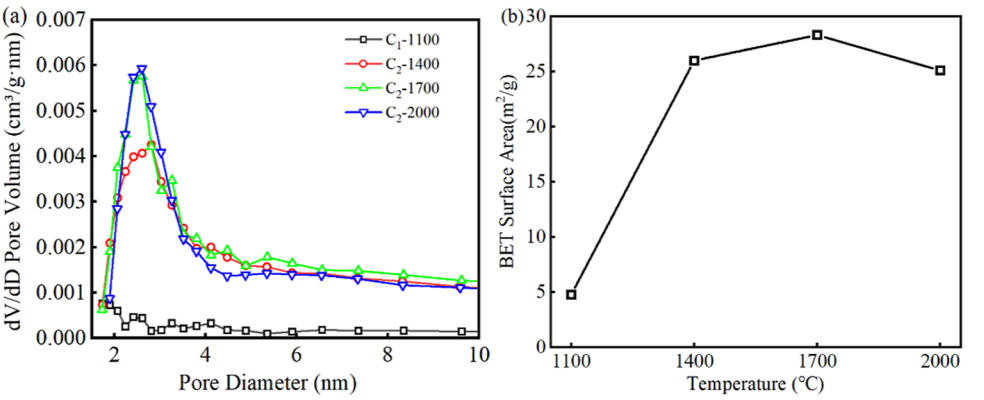

Figure 5. Pore structure and BET surface area of carbon black at different temperatures. (a) Aperture distribution curve. (b) Specific surface area changes curve of different carbon black samples.

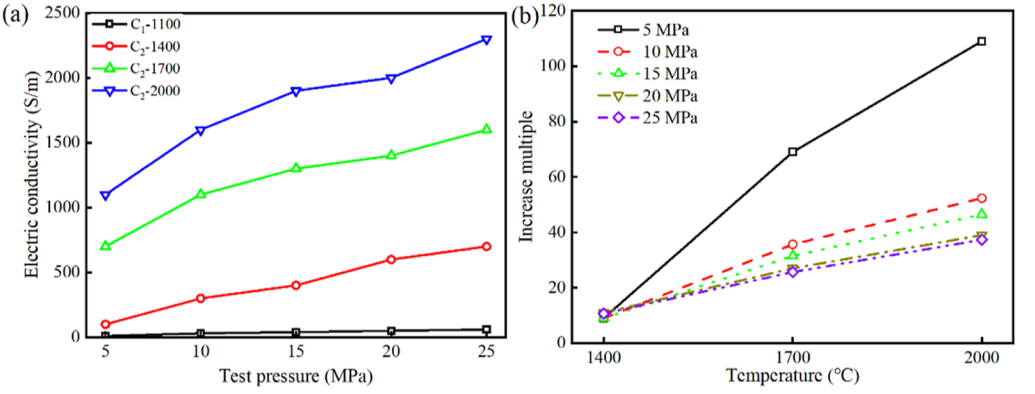

Figure 6. Electrical conductivity and electrical conductivity increase multiple (relative to C_1-1100) curves of carbon black at various test pressures and temperatures. (a) Carbon black electrical conductivity. (b) Carbon black electrical conductivity increase multiple.

https://doi.org/10.1021/acs.langmuir.4c03818
Langmuir XXXX, XXX, XXX−XXX

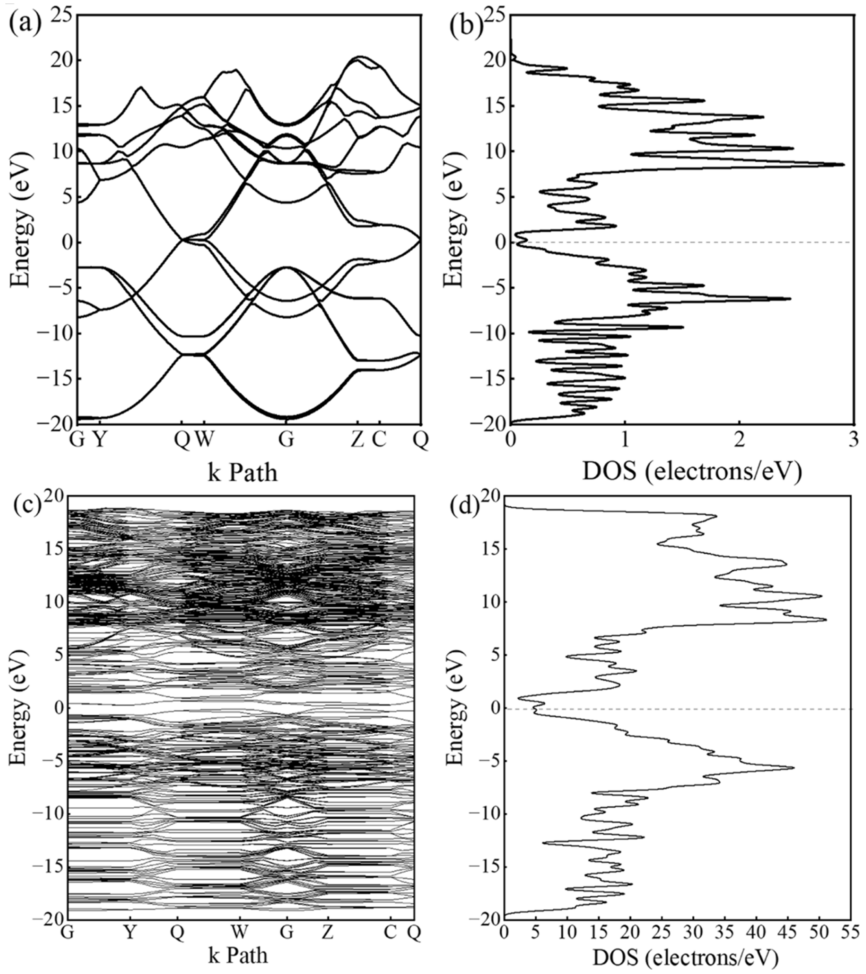

Figure 7. Band structure and state density of modified carbon black. (a) Band structure of defect-free carbon black. (b) State density of defect-free carbon black. (c) Band structure of carbon black with double-vacancy defects. (d) State density of carbon black with double-vacancy defects.

interlayer spacing of graphite. The result indicates that a rapid temperature increase and high-temperature conditions can promote a more refined and orderly rapid stacking of carbon atoms, which is conducive to the formation of a carbon structure with three-dimensional order similar to graphite. Additionally, apart from the distinct 002 and 100 peaks observed near 26° and 43°, respectively, peaks at 60°, 70°, and 77° corresponding to the 103, 104, and 110 planes also provide information regarding the grain size and stacking mode of the carbon material.[37] Particularly at 2000 °C, the intensity of these three peaks is more pronounced, indicating that the C_2-2000 sample has a higher degree of crystallinity. Furthermore, the thermal treatment process is accompanied by the growth and stacking of carbon black crystallites, as evidenced by an increase in the crystallite thickness L_c from 1.863 nm to 9.053 nm and an expansion in the lateral crystallite size L_a from 4.155 nm to 15.268 nm.

In Figure 4a, the Raman spectrum shows two bands at 1350 cm^{-1} (D band) and 1580 cm^{-1} (G band), which are denoted in Figure 4b, the former corresponding to disordered structure within the graphene planes and the latter associated with the in-plane vibrational motion of carbon atoms in sp^2-bonded atoms,[38] representing the information on graphitic carbon. The height, shape, position, and area of the D and G peaks of carbon black also have a certain impact on the final carbon structural properties.[39] The height and sharpness of the G peak indicate the presence of graphite carbon crystals. In contrast, a larger and broader D peak is associated with a higher degree of disordered carbon and defects in graphite materials. At 2000 °C, the C_2-2000 sample clearly has the sharpest D and G peaks, indicating that carbon black has the highest degree of graphitization at this temperature. Simultaneously, in the first-order spectrum, the D peak is fitted into four distinct peaks: the D_1 peak (~1360 cm^{-1}) indicative of defects in the graphite microcrystalline plane, the D_2 peak (~1620 cm^{-1}) representing the graphene layer on the surface, the D_3 peak (~1500 cm^{-1}) characteristic of amorphous carbon, and the D_4 peak (~1180 cm^{-1}) arising from a disordered graphite lattice.[40] Figure 4b shows the Raman spectrum fitting diagram of C_2-2000 sample. Additionally, a distinct 2D peak located at 2680 cm^{-1} was observed in the C_2-2000 sample, indicating the highly ordered graphite layers within the carbon matrix,[41] suggesting that the carbon black at 2000 °C exhibits a pronounced layered structure. The intensity ratio of the D_1 peak to the G peak (I_{D1}/I_G) reflects the graphitization degree of carbon black, and the calculated I_{D1}/I_G values are shown in Figure 4c. With the temperature increase, the I_{D1}/I_G value of the carbon black samples decreases from 2.46 to 0.82, indicating higher orderliness at higher temperatures, consistent with the results calculated from XRD.

Figure 5 presents the BET analytical results for the modified carbon black sample, including the pore size distribution curve

https://doi.org/10.1021/acs.langmuir.4c03818
Langmuir XXXX, XXX, XXX−XXX

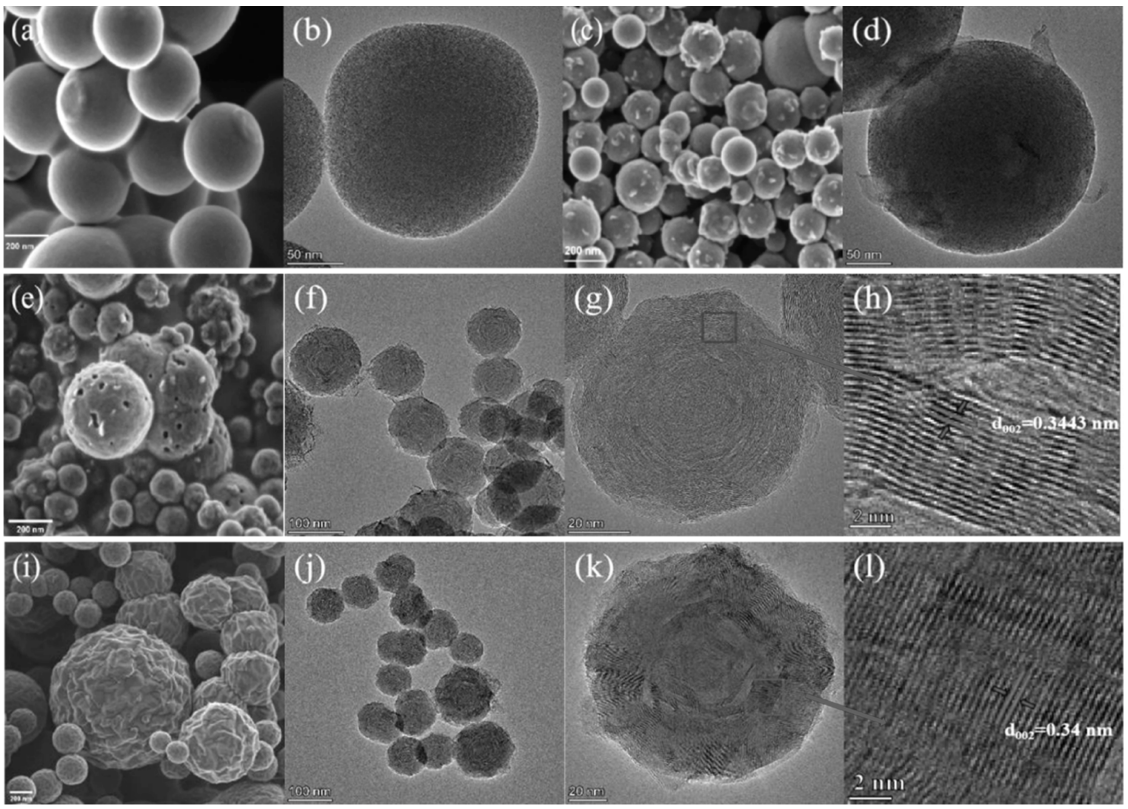

Figure 8. FESEM and TEM images of different carbon black samples. (a,b) C_1-1100. (c,d) C_2-1400. (e–h) C_2-1700. (i–l) C_2-2000. (a,c,e,i) FESEM images. (b,d,f–h,j–l) TEM images.

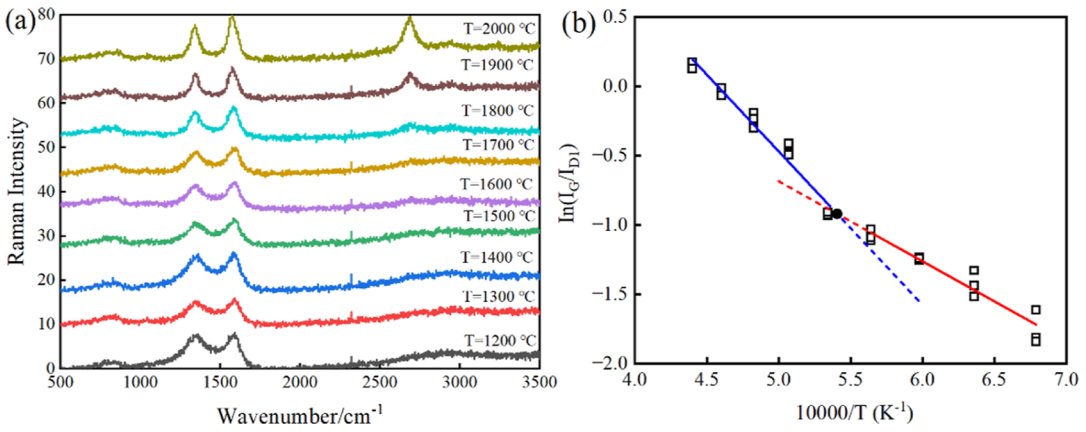

Figure 9. Structure analysis of modified carbon black samples at different temperatures. (a) Raman spectra and (b) relationship of I_G/I_{D1} with temperature.

and the specific surface area variation curve. While the temperature increases from 1100 to 1700 °C, carbon black restructures from the nonporous to the porous structure. The expansion of the pore size and the multiplication of pores contribute to the enlargement of the specific surface area of carbon black. However, when the temperature rises to 2000 °C, the abrupt decrease in the specific surface area, coupled with a reduction in the number of pores with diameters greater than 4 nm, indicates that the pores within the carbon black particles begin to shrink, resulting in a decrease in the specific surface area. In conjunction with the analyses from the XRD and Raman results, the phenomenon can be deduced as a further reduction in the interlayer spacing of carbon black particles and a decrease in the defect level within the particles. This results in contraction of the layered structure in the carbon black particle and a final reduction in the pore diameter.

3.2. Effect of Ordered Structure on Electrical Conductivity. The electrical conductivity of carbon black at various temperatures is presented in Figure 6. From Figure 6a, the electrical conductivity of carbon black gradually increases with the rise in temperature and test pressure. Under a pressure of 25 MPa, the electrical conductivity of the carbon black increases from 60 to 2300 S/m, falling within the range of the electrical conductivity of conductive carbon black (10^3 to 10^5 S/m). This suggests that the transformation of the defect structure in carbon black has enabled the transition from semiconductor properties to the properties of an excellent

https://doi.org/10.1021/acs.langmuir.4c03818
Langmuir XXXX, XXX, XXX–XXX

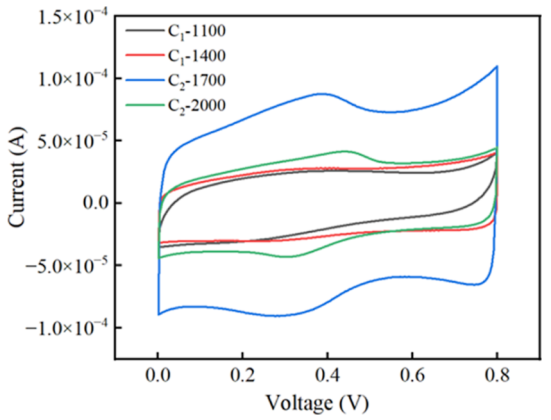

Figure 10. Cyclic voltammetry curves of carbon black at different temperatures.

conductive material. Figure 6b illustrates that while the carbon black exhibits a high electrical conductivity under high pressure, the increase multiple of conductivity decreases. This indicates that within the temperature range of 1400−2000 °C, the rate at which electrical conductivity increases with temperature is decelerating as the pressure increases.

The Raman test results indicate that the degree of defects in carbon black decreases with the increase in temperature. Therefore, the structural changes of carbon black at high temperature can be represented by the double-vacancy defect structure and the defect-free structure, thereby determining how the structure of carbon black affects electrical conductivity.[42,43] The band structure and density of states (DOS) calculations for carbon black with a defect-free structure and double-vacancy defect structure are shown in Figure 7. The band structure diagram in Figure 7a demonstrates that carbon black with a defect-free structure has a bandgap of zero, allowing valence electrons to more readily transition to the conduction band, suggesting that this structure of carbon black possesses good electrical conductivity. The DOS diagram in Figure 7b demonstrates that the DOS curve for carbon black has very sharp peaks, and the Fermi level intersects with the DOS curve. This further suggests that the defect-free structure of carbon black possesses metallic properties and exhibits good electrical conductivity. The band structure diagram in Figure 7c indicates that the bandgap of the carbon black increases from 0 to 0.208 electron volts, creating a forbidden band between the conduction and valence bands, where valence electrons require more energy to transition to the conduction band. The DOS diagram in Figure 7d shows that the curve of the carbon black becomes relatively flat and displays discontinuity near the Fermi level. This suggests that carbon black with double-vacancy defects has reduced electrical conductivity, endowing the material with enhanced semiconductor properties.

3.3. Morphological Characteristics of Modified Carbon Black Microcrystalline. Figure 8 shows the FESEM and TEM images of carbon black samples before and after modification. Carbon black particles are mainly observed to exist as irregular aggregates, with numerous branching

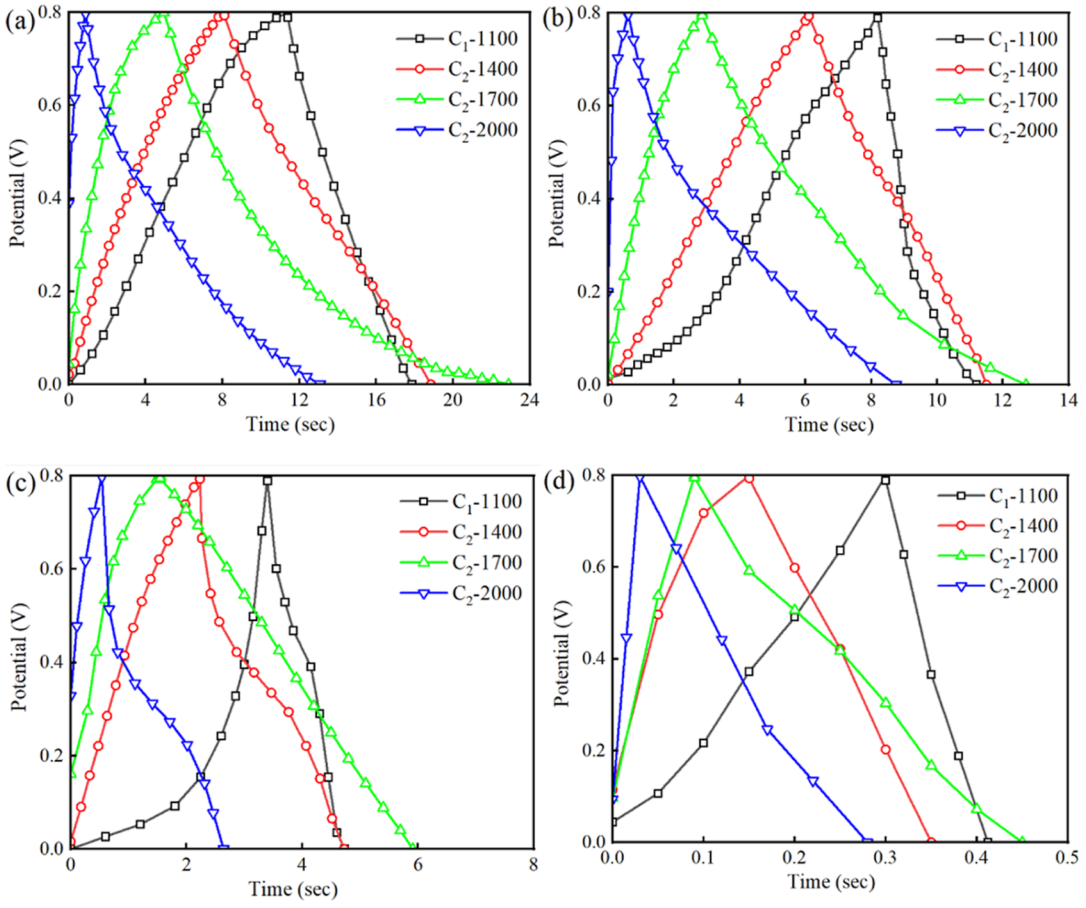

Figure 11. Constant current charge/discharge curve of carbon black under different load currents. (a) 0.5 A/g. (b) 1 A/g. (c) 2 A/g. (d) 20 A/g.

https://doi.org/10.1021/acs.langmuir.4c03818
Langmuir XXXX, XXX, XXX−XXX

Table 3. Specific Capacity of Carbon Black Samples at Different Temperatures

sample	C_1-1100	C_2-1400	C_2-1700	C_2-2000	acetylene carbon black (acetylene vapor deposition, 700 °C, nickel catalyst)[45]	KOH-activated sewage sludge (400 °C)[46]
C (F/g) 0.5 A/g	4.03	6.77	11.34	7.65	8.40	11.18
C (F/g) 1 A/g	3.75	6.51	11.11	7.45	8.10	10.76
C (F/g) 2 A/g	3.33	6.29	10.76	7.32	7.60	10.31
C (F/g) 20 A/g	2.80	5.00	9.00	6.25		
ΔC_1 (%)	17.37	7.09	5.12	4.31	9.52	7.78
ΔC_2 (%)	30.52	26.14	20.63	18.31		

structures forming on the surface. The branching increases the contact area for charge transfer and improves the rate of charge transfer. From Figure 8a,b, the carbon black particles in the initial sample are observed to be primarily spherical, with no surface porosity present. When the temperature is increased to 1400 °C, the carbon black surface no longer exhibits a complete spherical shape. As shown in Figure 8c, the C_1-1400 sample surface has developed fine particles. From the TEM image of the C_1-1400 sample in Figure 8d, distinct whisker-like particles are observed on the surface of the carbon black sample. The removal of volatile components at high temperatures causes the rupture and partial detachment of the surface disordered carbon. This leads to an increase in the original porous structure of the carbon black and the creation of additional specific surface area through the formation of whisker-like particles from the separated disordered carbon. Consequently, under the combined effects of the reduction in carbon black particle size and the formation of whisker-like particles on the surface, the specific surface area of the carbon black samples shows a sharp increase at temperatures between 1100 and 1400 °C. When the temperature continues to increase to 1700 °C, as shown in the FESEM diagram of the sample C_2-1700 in Figure 8e, a large number of pores appear on the surface of sample C_2-1700, thus forming porous spherical particles and resulting in a rapid increase in the surface area of carbon black. However, when the temperature rises to 2000 °C, as shown in the FESEM diagram of sample C_2-2000 in Figure 8i, the carbon black particles begin to close, the surface pores begin to shrink, and the specific surface area of carbon black decreases.

Figure 8f–h,j–l displays the TEM images of the modified carbon black samples at 1700 °C and 2000 °C, respectively. Figure 8h and Figure 8l are local magnifications of Figure 8g and Figure 8k, respectively. With the temperature rising further, the carbon atoms tend to arrange themselves into an orderly layered structure, and the crystallite size of carbon black gradually increases. From Figure 8g,h, the C_2-1700 carbon black sample shows a clear layering phenomenon on the particle surface. The interlayer spacing d_{002} aligns with the results from XRD measurements with both being approximately 0.345 nm. When the temperature further increases to 2000 °C, as shown in Figure 8k,l, the thermal expansion effect leads to a further reduction in the interlayer spacing of the carbon black internal crystallites. The d_{002} of the C_2-2000 carbon black sample decreased to around 0.34 nm. In addition, due to collision fusion of crystallites, transformation of disordered carbon, and an increase in the number of layers, the carbon black crystallite sizes L_a and L_c further increase.

3.4. Carbon Structure and Graphitization. Based on the analysis of the carbon black structure at different temperatures, the graphitization process of carbon black at high temperatures can be obtained. The initial carbon black particles are spherical particles and exist in the form of chain aggregates. With the increase in temperature, carbon black first experienced the process of surface disordered carbon shedding under the influence of volatilization and thermal stress. At 1400 °C, a large number of unshed disordered carbon layers appeared on the surface of carbon black, forming irregular spherical particles, carbon black particles with more pores began to form, and the particle size of carbon black particles also began to shrink, but no obvious layered ordered structure appeared. With the temperature further increasing, the amorphous carbon layers on the surface of carbon black particles essentially delaminate, forming a porous spherical particle structure. The amorphous structure within carbon black begins to transition into an ordered layered structure, with a further reduction in both particle diameter and interlayer spacing. At 1700 °C, carbon black particles formed an obvious multilayer graphite structure. When the temperature rapidly increases to 2000 °C, the interlayer spacing of the carbon black continues to decrease due to the thermal expansion effect, and the pores on the surface of the particles begin to close. Additionally, due to the collision fusion between carbon black grains and the increase in the number of layers, as well as the further transformation of disordered carbon, this leads to a rapid increase in the L_a and L_c dimensions of the carbon black crystals.

In order to determine the temperature limit of disordered carbon removal of carbon black and the formation of layered structures, samples C_1-1100 were taken as raw materials and left for 1 s at 1200–2000 °C, respectively. The Raman results are shown in Figure 9. The change rate of I_G/I_{D1} at different temperatures is taken as the graphitization rate of carbon black. The relationship between carbon black graphitization rate and temperature can be obtained by combining the Arrhenius equation. Through linear fitting of the data from the low- and high-temperature regions, the extrapolated lines intersect at a single point, corresponding to a temperature of 1576 °C. Thereby, the influence process of temperature on carbon black graphitization can be obtained. At temperatures between 1100 °C and 1576 °C, carbon black primarily undergoes the loss of disordered carbon, resulting in the formation of a porous carbon structure. Between 1576 °C and 2000 °C, a layered, ordered structure is formed, with the porosity gradually decreasing.

3.5. Performance of Modified Carbon Black in Supercapacitors. The cyclic voltammetry curves of all carbon black samples are shown in Figure 10. The CV curves of the carbon black samples tend to be rectangular in shape, consistent with the CV curve shape of the supercapacitors. The area enclosed by the CV curve represents the specific capacitance of carbon black. From the graph, the specific

https://doi.org/10.1021/acs.langmuir.4c03818
Langmuir XXXX, XXX, XXX–XXX

capacitance of carbon black peaks at 1700 °C. According to the BET characterization results, the specific capacitance of the carbon black increases with the increase in specific surface area when the temperature is between 1100 °C and 1700 °C. However, when the temperature is raised to 2000 °C, the specific surface area of the sample C_2-2000 is lower than that of the sample C_2-1400, yet the specific capacitance of C_2-2000 is higher than that of C_2-1400. The enhancement of porosity facilitates the diffusion of charge within carbon black and expands the space available for charge storage, thereby increasing the specific capacitance of carbon black. Consistent with the literature on the correlation between specific capacitance and the specific surface area and conductivity of carbon material,[44] the carbon black's high specific surface area and porosity contribute to the elevated specific capacitance.

Based on the constant current charge−discharge curves illustrated in Figure 11, the specific capacitance values for each carbon black sample under different current loads are calculated and listed in Table 3. The sample C_2-1700 exhibits the highest specific capacitance, reaching 11.34 F/g, primarily due to the porous structure characteristics compared with other modified carbon black samples. The high specific surface area and porosity afforded by the porous structure are conducive to the storage and transport of charge. The capacitance decrement percentages are ascertained for both high and extreme current loads with ΔC_1 (%) corresponding to 2 A/g and ΔC_2 (%) corresponding to 20 A/g. Observing the constant current charging curves, the charging time within the capacitor decreases noticeably with the increase in the heat treatment temperature of the carbon black, aligning with the changes in electrical conductivity of carbon black. The enhanced orderliness of the carbon black significantly improves electrical conductivity, which in turn increases the charging rate of the capacitor. The sample C_2-2000, characterized by good crystallinity and order, shows the smallest decrease in capacitance compared to the sample C_1-1100, which has obvious structural defects, with only a 4.31% decrease at the high current load of 2 A/g and an 18.31% decrease at the extreme current load of 20 A/g. This indicates that C_2-2000 has a stable electrochemical performance. However, excessively high temperatures can cause the closure of surface pores on carbon black particles, which may lead to a reduction in specific capacitance. Therefore, these particles must undergo an activation process to improve performance in supercapacitors.

4. CONCLUSIONS

The pyrolytic carbon black is subjected to high-temperature modification treatment at 1400 °C, 1700 °C, and 2000 °C using ultrafast Joule heating technology. At 1100−1576 °C, with the increase of temperature, carbon black particles form a porous structure due to the partially disordered carbon falling off, resulting in an increase in the specific surface area of carbon black particles, and the carbon black particles gradually change to a layered structure. Upon reaching a temperature of 1700 °C, a pronounced multilayered structure characteristic of graphite was observed to form. With the temperature rising to 2000 °C, the interplanar spacing within the carbon black particles was observed to decrease, concurrently with an increase in the number of layers. The electrical conductivity of these carbon black particles was enhanced to a level of 2300 S/m. Under a high current load of 2 A/g, the observed capacitance reduction was a mere 4.31%, and under the more extreme current load of 20 A/g, the capacitance reduction was limited to 18.31%. Therefore, a potential supercapacitor material had been offered, with modified carbon black serving as the electrode material.

AUTHOR INFORMATION

Corresponding Authors

Zhongjie Shen − *National Energy Coal Gasification Technology Research and Development Center, East China University of Science and Technology, Shanghai 200237, P. R. China; Shanghai Engineering Research Center of Coal Gasification, East China University of Science and Technology, Shanghai 200237, P. R. China;* orcid.org/0000-0002-7140-1843; Phone: +86 21 64253933; Email: zjshen@ecust.edu.cn

Haifeng Liu − *National Energy Coal Gasification Technology Research and Development Center, East China University of Science and Technology, Shanghai 200237, P. R. China; Shanghai Engineering Research Center of Coal Gasification, East China University of Science and Technology, Shanghai 200237, P. R. China; Liaoning Petrochemical University, Fushun, Liaoning 113001, PR. China*; Phone: +86 21 64251418; Email: hfliu@ecust.edu.cn

Author

Guinan He − *National Energy Coal Gasification Technology Research and Development Center, East China University of Science and Technology, Shanghai 200237, P. R. China; Shanghai Engineering Research Center of Coal Gasification, East China University of Science and Technology, Shanghai 200237, P. R. China*

Complete contact information is available at: https://pubs.acs.org/10.1021/acs.langmuir.4c03818

Author Contributions

Guinan He: resources, data curation, formal analysis, investigation, methodology, software, visualization, writing—original draft, writing—review and editing. Zhongjie Shen: conceptualization, supervision, formal analysis, methodology, software, writing—review and editing, project administration, funding acquisition. Haifeng Liu: conceptualization, supervision, validation, formal analysis, methodology.

Notes

The authors declare no competing financial interest.

Print declaration: all figures are in color in the online version and black/white in print.

ACKNOWLEDGMENTS

This study was supported by the National Natural Science Foundation of China (22378130) and the Fundamental Research Funds of the Central Universities (2022ZFJH004).

REFERENCES

(1) Gielen, D.; Boshell, F.; Saygin, D.; Bazilian, M. D.; Wagner, N.; Gorini, R. The role of renewable energy in the global energy transformation. *Energy Strategy Rev.* **2019**, *24*, 38−50.

(2) Yang, Z.; Zhang, J.; Kintner-Meyer, M. C. W.; Lu, X.; Choi, D.; Lemmon, J. P.; Liu, J. Electrochemical energy storage for green grid. *Chem. Rev.* **2011**, *111*, 3577−3613.

(3) Engeland, K.; Borga, M.; Creutin, J. D.; François, B.; Ramos, M. H.; Vidal, J. P. Space-time variability of climate variables and intermittent renewable electricity production − A review. *Renewable Sustainable Energy Rev.* **2017**, *79*, 600−617.

https://doi.org/10.1021/acs.langmuir.4c03818
Langmuir XXXX, XXX, XXX−XXX

(4) Fu, T.; Zhang, B.; Gao, X.; Cui, S.; Guan, C. Y.; Zhang, Y.; Zhang, B.; Peng, Y. Recent progresses; challenges; and opportunities of carbon-based materials applied in heavy metal polluted soil remediation. *Sci. Total Environ.* **2023**, *856*, 158810.
(5) Wang, F.; Wu, X.; Yuan, X.; Liu, Z.; Zhang, Y.; Fu, L.; Zhu, Y.; Zhou, Q.; Wu, Y.; Huang, W. Latest advances in supercapacitors: from new electrode materials to novel device designs. *Chem. Soc. Rev.* **2017**, *46*, 6816−6854.
(6) Shao, Y.; El-Kady, M. F.; Sun, J.; Li, Y.; Zhang, Q.; Zhu, M.; Wang, H.; Dunn, B.; Kaner, R. B. Design and mechanisms of asymmetric supercapacitors. *Chem. Rev.* **2018**, *118*, 9233−9280.
(7) Poonam; Sharma, K.; Arora, A.; Tripathi, S. K. Review of supercapacitors: Materials and devices. *J. Energy Storage* **2019**, *21*, 801−825.
(8) Wang, Y.; Zhang, L.; Hou, H.; Xu, W.; Duan, G.; He, S.; Liu, K.; Jiang, S. Recent progress in carbon-based materials for supercapacitor electrodes: a review. *J. Mater. Sci.* **2021**, *56*, 173−200.
(9) Simon, P.; Gogotsi, Y. Perspectives for electrochemical capacitors and related devices. *Nat. Mater.* **2020**, *19*, 1151−1163.
(10) Chen, C. C.; Huang, Y. H.; Chien, H. J. Waste tire-derived porous nitrogen-doped carbon black as an electrode material for supercapacitors. *Sustainable Chem. Pharm.* **2021**, *24*, 100535.
(11) Chen, G.; Yu, X.; Ostrikov, K.; Liu, B.; Harding, J.; Homm, G.; Guo, H.; Andreas Schunk, S.; Zhou, Y.; Tu, X.; et al. Methane up-carbonizing: A way towards clean hydrogen energy? *Chem. Eng. J.* **2023**, *476*, 146335.
(12) Zhou, J.; Zhao, J.; Zhang, J.; Zhang, T.; Ye, M.; Liu, Z. Regeneration of Catalysts Deactivated by Coke Deposition: A Review. *Chin. J. Catal.* **2020**, *41* (7), 1048−1061.
(13) Chan, Y. H.; Chan, Z. P.; Lock, S. S. M.; Yiin, C. L.; Foong, S. Y.; Wong, M. K.; Ishak, M. A.; Quek, V. C.; Ge, S.; Lam, S. S. Thermal pyrolysis conversion of methane to hydrogen (H_2): A review on process parameters; reaction kinetics and techno-economic analysis. *Chin. Chem. Lett.* **2024**, *35*, 109329.
(14) Patlolla, S. R.; Katsu, K.; Sharafian, A.; Wei, K.; Herrera, O. E.; Mérida, W. A review of methane pyrolysis technologies for hydrogen production. *Renewable Sustainable Energy Rev.* **2023**, *181*, 113323.
(15) Zhai, Z.; Zhang, L.; Du, T.; Ren, B.; Xu, Y.; Wang, S.; Miao, J.; Liu, Z. A review of carbon materials for supercapacitors. *Mater. Des.* **2022**, *221*, 111017.
(16) Chen, K.; Li, L. Ordered structures with functional units as a paradigm of material design. *Adv. Mater.* **2019**, *31*, 1901115.
(17) Reddy, S. S.; Sinha, A. K.; Amarendra, G.; Shekar, N. V. C.; Bhalerao, G. M. Enhancement of graphitic order in carbon black using precursor additive. *Diamond Relat. Mater.* **2020**, *101*, 107539.
(18) Chen, C.; Sun, K.; Huang, C.; Yang, M.; Fan, M.; Wang, A.; Zhang, G.; Li, B.; Jiang, J.; Xu, W.; et al. Investigation on the mechanism of structural reconstruction of biochars derived from lignin and cellulose during graphitization under high temperature. *Biochar* **2023**, *5*, 51.
(19) Feng, W.; Qin, M.; Feng, Y. Toward highly thermally conductive all-carbon composites: Structure control. *Carbon* **2016**, *109*, 575−597.
(20) Ouzilleau, P.; Gheribi, A. E.; Chartrand, P. The graphitization temperature threshold analyzed through a second-order structural transformation. *Carbon* **2016**, *109*, 896−908.
(21) Khodabakhshi, S.; Fulvio, P. F.; Andreoli, E. Carbon black reborn: Structure and chemistry for renewable energy harnessing. *Carbon* **2020**, *162*, 604−649.
(22) Zhang, X.; Mao, Q.; You, Z.; Song, Y.; Wan, Y.; Xiao, J.; Zhong, Q. Construction of a 3D "onion-like" model of conductive carbon black for lithium-ion batteries and exploration of the electrochemical oxidation mechanism of CB and ethylene carbonate via ReaxFF MD. *Energy Fuels* **2023**, *37*, 6778−6790.
(23) Kim, D. W.; Kil, H. S.; Kim, J.; Mochida, I.; Nakabayashi, K.; Rhee, C. K.; Miyawaki, J.; Yoon, S. H. Highly graphitized carbon from non-graphitizable raw material and its formation mechanism based on domain theory. *Carbon* **2017**, *121*, 301−308.
(24) Zhao, J.; Yang, L.; Li, F.; Yu, R.; Jin, C. Structural evolution in the graphitization process of activated carbon by high-pressure sintering. *Carbon* **2009**, *47*, 744−751.
(25) Wang, Y.; Yang, L.; Wang, Y.; Wu, Y.; Li, S.; Cao, B.; Qiao, Y.; Ren, G.; Zhou, T.; Chen, Y. Boron-doped polyhedral graphite catalyzed by h-BN via structural induction for lithium storage. *Carbon* **2024**, *226*, 119175.
(26) Yin, Y. C.; Li, C.; Hu, X.; Zuo, D.; Yang, L.; Zhou, L.; Yang, J.; Wan, J. Rapid direct regeneration of spent $LiCoO_2$ cathodes for Li-ion batteries. *ACS Energy Lett.* **2023**, *8*, 3005−3012.
(27) Ding, X.; He, Z.; Li, J.; Xu, X.; Li, Z. Carbon carrier-based rapid Joule heating technology: a review on the preparation and applications of functional nanomaterials. *Nanoscale* **2024**, *16*, 12309−12328.
(28) Chen, Y. *High temperature shock technology: Ultra-fast micro-nano manufacturing*; Springer Nature, 2023.
(29) Lu, M.; Liang, L.; Feng, B.; Chang, Y.; Huang, Z.; Song, H.; Du, L.; Liao, S.; Cui, Z. Ultrafast carbothermal shock strategy enabled highly graphitic porous carbon supports for fuel cells. *Chin. J. Catal.* **2023**, *52*, 228−238.
(30) Jiang, F.; Yao, Y.; Natarajan, B.; Yang, C.; Gao, T.; Xie, H.; Wang, Y.; Xu, L.; Chen, Y.; Gilman, J.; et al. Ultrahigh-temperature conversion of biomass to highly conductive graphitic carbon. *Carbon* **2019**, *144*, 241−248.
(31) Luong, D. X.; Bets, K. V.; Algozeeb, W. A.; Stanford, M. G.; Kittrell, C.; Chen, W. W.; Salvatierra, R. V.; Ren, M.; McHugh, E. A.; Advincula, P. A.; et al. Gram-scale bottom-up flash graphene synthesis. *Nature* **2020**, *577*, 647−651.
(32) Chen, W.; Li, J. T.; Wang, Z.; Algozeeb, W. A.; Luong, D. X.; Kittrell, C. C.; McHugh, E. A.; Advincula, P. A.; Wyss, K. M.; Beckham, J. L.; et al. Ultrafast and controllable phase evolution by flash joule heating. *ACS Nano* **2021**, *15*, 11158−11167.
(33) Holzwarth, U.; Gibson, N. The Scherrer equation versus the "Debye-Scherrer equatio. *Nat. Nanotechnol.* **2011**, *6*, 534.
(34) Yang, C.; Li, D. Flexible and foldable supercapacitor electrodes from the porous 3D network of cellulose nanofibers; carbon nanotubes and polyaniline. *Mater. Lett.* **2015**, *155*, 78−81.
(35) Kohn, W.; Sham, L. J. Self-consistent equations including exchange and correlation effects. *Phys. Rev.* **1965**, *140*, A1133−A1138.
(36) Carmona-Espíndola, J.; Gázquez, J. L.; Vela, A.; Trickey, S. B. Generalized gradient approximation exchange energy functional with near-best semilocal performance. *J. Chem. Theory Comput.* **2019**, *15*, 303−310.
(37) Ben Amor, A.; Hemmami, H.; Gherbi, M. T.; Seghir, B. B.; Zeghoud, S.; Gharbi, A. H.; Chenna, D.; Ben Amor, I.; Alsaeedi, H.; Cornu, D.; Bechelany, M.; Barhoum, A. Synthesis of Spherical Carbon Nanoparticles from Orange Peel and Their Surface Modification with Chitosan: Evaluation of Optical Properties, Biocompatibility, Antioxidant and Anti-Hemolytic Activity. *Biomass Convers. Biorefin.* **2024**.
(38) Wang, Y.; Serrano, S.; Santiago-Avilés, J. J. Raman characterization of carbon nanofibers prepared using electrospinning. *Synth. Met.* **2003**, *138*, 423−427.
(39) Ferrante, C.; Virga, A.; Benfatto, L.; Martinati, M.; De Fazio, D.; Sassi, U.; Fasolato, C.; Ott, A. K.; Postorino, P.; Yoon, D.; Cerullo, G.; Mauri, F.; Ferrari, A. C.; Scopigno, T. Raman Spectroscopy of Graphene under Ultrafast Laser Excitation. *Nat. Commun.* **2018**, *9* (1), 308.
(40) Sadezky, A.; Muckenhuber, H.; Grothe, H.; Niessner, R.; Pöschl, U. Raman microspectroscopy of soot and related carbonaceous materials: Spectral analysis and structural information. *Carbon* **2005**, *43*, 1731−1742.
(41) Jin, M.; Cheng, L.; Zheng, W.; Ding, Y.; Zhu, Y.; Jia, L.; Huang, F. Raman tensor of graphite: Symmetry of G; D and D′ phonons. *Sci. China Mater.* **2022**, *65*, 268−272.
(42) De Souza, L. A.; Monteiro De Castro, G.; Marques, L. F.; Belchior, J. C. A DFT investigation of lithium adsorption on graphenes as a potential anode material in lithium-ion batteries. *J. Mol. Graphics Modell.* **2021**, *108*, 107998.

https://doi.org/10.1021/acs.langmuir.4c03818
Langmuir XXXX, XXX, XXX−XXX

(43) Tao, L. Q.; Zou, S.; Wang, G.; Peng, Z.; Zhu, C.; Sun, H. Theoretical analysis of the absorption of CO_2 and CO on pristine and Al-doped C_3B. *Phys. Chem. Chem. Phys.* **2022**, *24*, 27224−27231.
(44) Mosch, H. L. K. S.; Akintola, O.; Plass, W.; Höppener, S.; Schubert, U. S.; Ignaszak, A. Specific Surface versus Electrochemically Active Area of the Carbon/Polypyrrole Capacitor: Correlation of Ion Dynamics Studied by an Electrochemical Quartz Crystal Microbalance with BET Surface. *Langmuir* **2016**, *32* (18), 4440−4449.
(45) Hulicova-Jurcakova, D.; Li, X.; Zhu, Z.; de Marco, R.; Lu, G. Q. Graphitic carbon nanofibers synthesized by the chemical vapor deposition (CVD) method and their electrochemical performances in supercapacitors. *Energy Fuels* **2008**, *22*, 4139−4145.
(46) Singh, A.; Srivastava, V. C.; Janowska, I. Utilization of carbon-black industry waste to synthesize electrode material for supercapacitors. *Energy Storage* **2024**, *6*, No. e677.

https://doi.org/10.1021/acs.langmuir.4c03818
Langmuir XXXX, XXX, XXX−XXX